Available online at www.sciencedirect.com
SCIENCE DIRECT
ELSEVIER
Journal of Molecular Catalysis A: Chemical 255 (2006) 123–130
JOURNAL OF MOLECULAR CATALYSIS A: CHEMICAL
www.elsevier.com/locate/molcata

Cobalt-containing hexagonal mesoporous molecular sieves (Co-HMS): Synthesis, characterization and catalytic activity in the oxidation reaction of ethylbenzene

Shrikant S. Bhoware, S. Shylesh, K.R. Kamble, A.P. Singh *

Inorganic and Catalysis Division, National Chemical Laboratory, Pune 411008, Maharashtra, India

Received 16 January 2006; accepted 31 March 2006
Available online 11 May 2006

Abstract

Cobalt-containing hexagonal mesoporous materials (Co-HMS and Co/HMS) with different cobalt content were synthesized for the first time by direct hydrothermal and post-synthesis (grafting) method. The materials were characterized in detail by X-ray diffraction, BET surface area, N_2 sorption isotherms, SEM, TEM, UV–vis and XPS techniques. Powder X-ray diffraction pattern, N_2 adsorption–desorption analysis and TEM analysis show the presence of hexagonal mesoporous structure, having Type IV isotherms and reveals the typical wormhole-like morphology. Spectroscopic techniques like UV–vis and XPS reveal cobalt in +2 oxidation state and tetrahedrally coordinated. Liquid phase oxidation of ethylbenzene using TBHP (70 wt%) as an oxidant shows that the catalysts are highly active, under solvent free conditions as well as under lower cobalt concentrations. Leaching studies performed by hot filtration experiments show that the cobalt catalysts prepared by hydrothermal methods are stable, while the grafted catalysts show the leaching of cobalt under the reaction conditions.

Keywords: HMS; Co-HMS; Hydrothermal; Ethylbenzene; Oxidation

1. Introduction

Discovery of silica based family of mesoporous materials, designated as M41S, in last decade by Mobile Oil Corporation has attracted great attention because it extends the range of molecular sieves materials into the varied large pore regime [1,2]. The pore size of the materials can be tuned by controlling the chain length of the structure-directing agent or by using auxiliary solvent co-surfactant to swell the micelles. In another approach, neutral templating mechanism (S°I°) was followed to prepare mesoporous molecular sieves that are based on hydrogen bonding and self-assembly between neutral primary amine surfactant (S°) and neutral inorganic precursor (I°) [3,4]. This neutral S°I° templating route afforded a distinguishable subset of hexagonal molecular sieves, designated as HMS [3]. Unlike MCM-41, HMS materials lack higher order Bragg reflections in the XRD patterns while the electron diffraction patterns showed that they possessed hexagonal symmetry similar to MCM-41. Tanev et al. reported the synthesis of titanium containing hexagonal mesoporous silica (Ti-HMS) by using neutral amine surfactant for the first time and shown its high catalytic activity than the Ti-MCM-41 catalysts for bulky substrates [3]. Compared to conventional microporous zeolite, mesoporous materials possess many advantages such as high surface area, large pore size, narrow pore size distribution, and an ordered structure. However, the amorphous framework and the lack of active centers in the pure silica mesoporous material limited their direct application. As a result, more research work concerning mesoporous material has been focused on enhancing their reactivity through chemical modification. Synthetic routes exploit the advantageous properties of mesoporous silica by the isomorphous substitution, impregnation, grafting and encapsulation of metal and metal complexes. The identification and implementations of effective catalytic systems for liquid phase oxidation, particularly in the manufacturing of fine chemicals is considered to be one of the major target of chemical industries. The need for such a system is widely accepted, specifically to replace inorganic oxidant that are using stoichiometric amounts and possessing handling and

* Corresponding author. Tel.: +91 2025893761; fax: +91 2025893761.
E-mail address: ap.singh@ncl.res.in (A.P. Singh).

1381-1169/$ – see front matter © 2006 Elsevier B.V. All rights reserved.
doi:10.1016/j.molcata.2006.03.072

environmental issues. Heterogeneous catalysts had many inherent advantages such as ease of recovery and recycling of the catalyst as well as suitable for continuous processing. A number of different strategies for the heterogenisation of the redox active elements are being explored and include framework substituted molecular sieves. Cobalt acts as a very good catalyst for Fischer–Tropsch reaction and had been further exploited for long chain hydrocarbon synthesis [5]. Besides this, its excellent performance in side chain oxidation of aromatics urged researchers to deal more about the redox properties. Until now, Ti, V, Al, B, Ga and Fe were successfully incorporated in the framework of HMS [6–8]. However, no literature was found on cobalt-substituted mesoporous HMS by direct synthesis method.

Herein we report for the first time, the synthesis and characterization of cobalt-containing hexagonal mesoporous silica (Co-HMS) materials prepared by two different synthetic routes and its catalytic activity evaluation in the liquid phase oxidation reaction of ethylbenzene.

2. Experimental

The silica source used was tetraethyl orthosilicate (TEOS) [$Si(OC_2H_5)_4$, 98%] obtained from Lancaster. Hexadecyl amine (HA) [$C_{16}H_{35}N$, 95%] was obtained from Aldrich. Ethyl alcohol [C_2H_5OH, 99.9%] was purchased from Merck. Cobalt acetylacetone [$Co(acac)_2$, 99%] was supplied by Across. All reagents were used as received without further purification.

2.1. Synthesis

2.1.1. Synthesis of cobalt-substituted hexagonal molecular sieves (Co-HMS)

Co-HMS was prepared by direct hydrothermal method using TEOS as the inorganic source and HA as the structure-directing agent. In a typical synthesis, in an ethyl alcohol–water mixture (14.8 and 100 g, respectively) hexadecyl amine (3.38 g) was added and stirred for 30 min at 30 °C. To this solution, TEOS (8.8 g) was added very slowly. After half an hour, an ethanolic solution of cobalt acetylacetone was poured into gel in a dropwise manner and stirring was further continued for 3 h (pH 7.2).

Molar gel composition of the final gel mixture was as follows,

$$1TEOS : xM : 0.33HA : 10.75EtOH : 139H_2O$$

where '*x*' is the calculated amount of cobalt for different Si/Co ratios. The gel was transferred into a glass bottle and kept in an oil bath at 100 °C for 48 h. It was then filtered, washed several times with deionized water and dried at 100 °C for 12 h. Finally, the material was calcined at 525 °C for 12 h and designated as Co-HMS (100), Co-HMS (80) and Co-HMS (50) for Si/Co ratios of 100, 80 and 50, respectively. For comparison, a pure siliceous HMS material was also synthesized by the same method but without the addition of cobalt acetylacteone.

2.1.2. Synthesis of cobalt-grafted hexagonal molecular sieves (Co/HMS)

Cobalt acetylacteone (0.09 and 0.18 g for 1 and 2 wt%) was dissolved in anhydrous toluene (100 g) and stirred for 1 h to make a homogenous solution. To this solution, 2 g of calcined HMS was added and stirred at 100 °C for 12 h. Thereafter the solvent was evaporated and calcined at 525 °C as stated in Section 2.1. The calcined material was designated as Co-HMS (1) and Co-HMS (2) for 1 and 2 wt% cobalt loading.

2.2. Characterization

Powder X-ray diffraction pattern of the samples were recorded on a Rigaku D max III VC Ni filtered Cu Kα radiation, $\lambda = 1.5404$ between 1 and 8 (2θ) with a scanning rate of 1° min^{-1}. The specific surface area, total pore volume and average pore diameter measured by the N_2 adsorption desorption method using NOVA 1200 (Quanta Chrome) instrument. The samples were activated at 300 °C for 3 h under vacuum and then adsorption desorption was conducted by passing nitrogen over samples which was kept under liquid nitrogen. Pore size distribution was obtained by applying BJH pore analysis method to the desorption branch of nitrogen adsorption isotherm. SEM micrograph of the cobalt-containing samples were obtained on JEOL-JSM 520 scanning microscope while the TEM images were performed on a JEOL-TEM 1200 EX instrument with 100 kV accelerating voltage to probe the mesoporosity of the material. Cobalt content in the samples was determined by atomic absorbance analysis using Perkin-Elmer 11013 spectrometer after dissolution of the samples in HCl–HF solution. Diffuse reflectance UV–vis spectra of the powder samples were recorded in the range 200–800 nm on Shimadzu UV 2101 PC spectrometer equipped with a diffuse reflectance attachment, using $BaSO_4$ as the reference. XPS measurements were performed on a VG Microtech ESCA 3000 instrument using non-monochromatized Mg Kα radiation at a pass energy of 50 eV and an electron take off angle of 60°. The correction of binding energy (B.E.) was performed by using the C_{1s} peak of carbon at 285 eV as reference.

2.3. Catalytic reaction

Oxidation reactions of ethylbenzene were performed in a round bottom flask fitted with a water condenser using *tert*-butyl hydrogen peroxide (TBHP, 70 wt%) as an oxidant. The reaction mixture of the ethylbenzene (1 g, 9.4 mmol) and TBHP (70 wt%, 1.22 g, 9.4 mmol) was added to catalyst (5 wt% with respect to ethylbenzene) and heated at constant temperature of 80 °C under magnetic stirring (Scheme 1). After reaction,

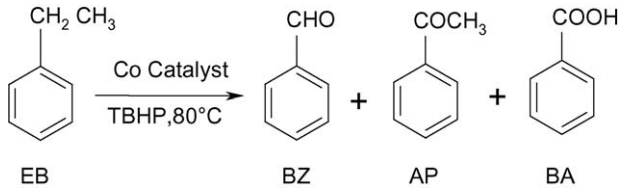

Scheme 1. Oxidation of ethylbenzene.

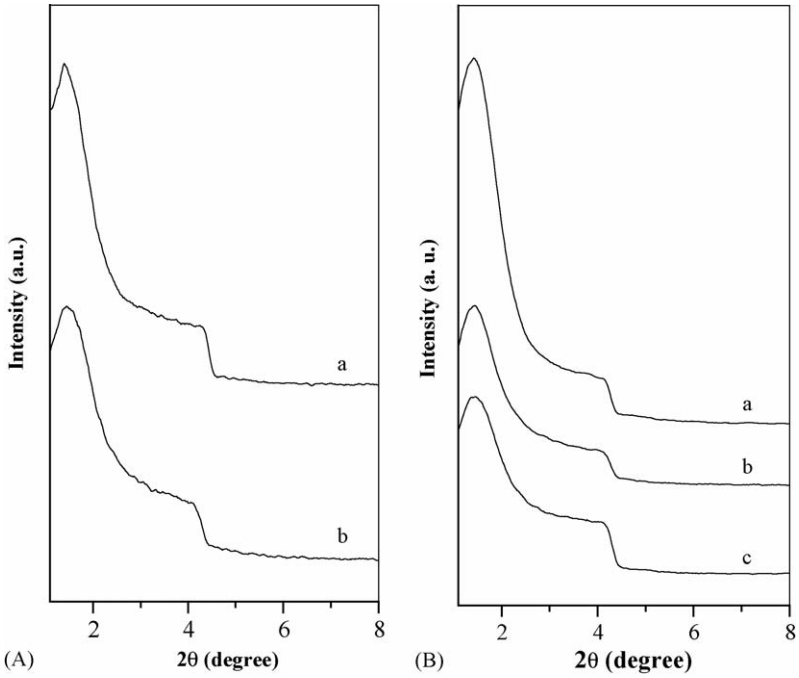

Fig. 1. Powder X-ray diffraction of calcined [A] (a) Co-HMS (100), (b) Co-HMS (50); [B] (a) HMS, (b) Co/HMS (1), (c) Co/HMS (2).

the reaction mixture was cooled to room temperature and the catalyst was separated by centrifugation. The products were analyzed by gas chromatograph (6890) equipped with a flame ionization detector (FID) and a capillary column (5 μm cross linked methyl silicone gun 0.2 mm × 50 m) and was further confirmed by GC–MS (Shimadzu 200A). Leaching of the metal during the course of reaction was verified by resubmission of the filtrate to the same reaction conditions.

3. Results and discussion

3.1. Powder X-ray diffraction

Fig. 1 shows the X- ray diffraction (XRD) pattern of calcined cobalt-substituted and grafted HMS samples with different amounts of cobalt. The XRD patterns are similar to the reports of Tanev et al. [3]. Unlike MCM-41 material, HMS shows only d_{100} reflection peak and the higher order Bragg's reflections are absent which suggests that the structure of the material is poorly ordered [9,10]. In Co-HMS samples, increasing cobalt amount results in a decrease in the intensity of d_{100} reflection peak and the peak gets broadened with a slight shift in 2θ angle towards lower value (Fig. 1A). Moreover, compared to pure HMS sample, the cobalt-containing samples show an increase in the d-spacing values (Table 1) and thereby increases the unit cell values. In cobalt-containing HMS, we observed that the d values are greater than reported value [3,8–10]. This phenomenon may be due to the high temperature hydrothermal synthesis performed in the present case, than the earlier reported room temperature synthesis. Indeed, Pauly and Pinnavaia claimed that with increase in synthesis temperature, pore–pore correlation distance systematically increased [9]. Contrary, in case of Co/HMS sample, with an increase in amount of cobalt loading the d_{100} reflection peak decreases with a corresponding shift to higher 2θ values due to accumulation of cobalt on the surface of the wall (Fig. 1B).

3.2. Nitrogen adsorption–desorption measurements

N_2 adsorption–desorption isotherms and pore size distribution curves, determined from the BJH method, of cobalt-containing HMS materials are shown in Figs. 2 and 3 and the

Table 1
Physical properties of cobalt-containing HMS catalyst

Entry	Catalyst[a]	Cobalt content[b] (wt%)	d_{100} (Å)	S_{BET} (m^2/g)	Pore volume V_p (cc/g)
1	HMS	–	62.11	503	1.32
2	Co-HMS (100)	0.98	62.39	538	1.29
3	Co-HMS (50)	1.90	62.47	618	1.20
4	Co/HMS (1)	1.05	61.74	485	1.25
5	Co/HMS (2)	1.97	61.52	462	1.17

[a] Co-HMS (100) and Co-HMS (50) stands for cobalt-containing HMS synthesized by direct hydrothermal method with Si/Co ratios 100 and 50, respectively. Co/HMS (1) and Co/HMS (2) stand for cobalt-containing HMS synthesized by post-synthesis method with 1 and 2 wt% cobalt loading, respectively.
[b] The Co content calculated by AAS.

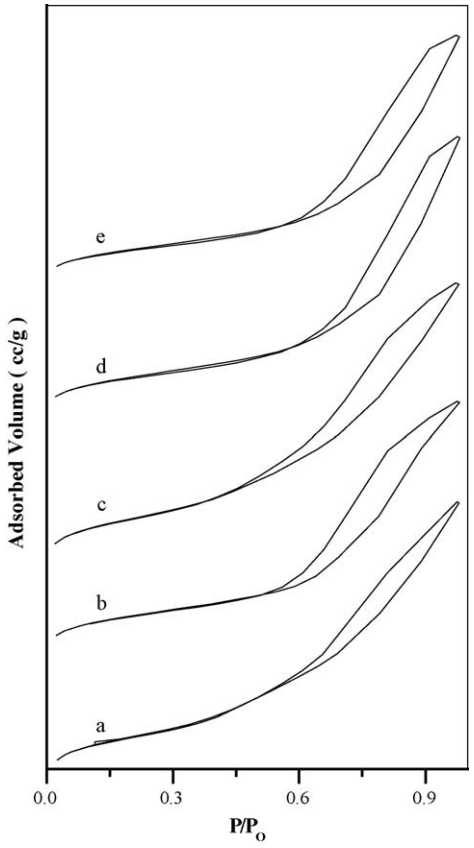

Fig. 2. N_2 adsorption desorption isotherms of: (a) HMS, (b) Co/HMS (1), (c) Co/HMS (2), (d) Co-HMS (100) and (e) Co-HMS (50).

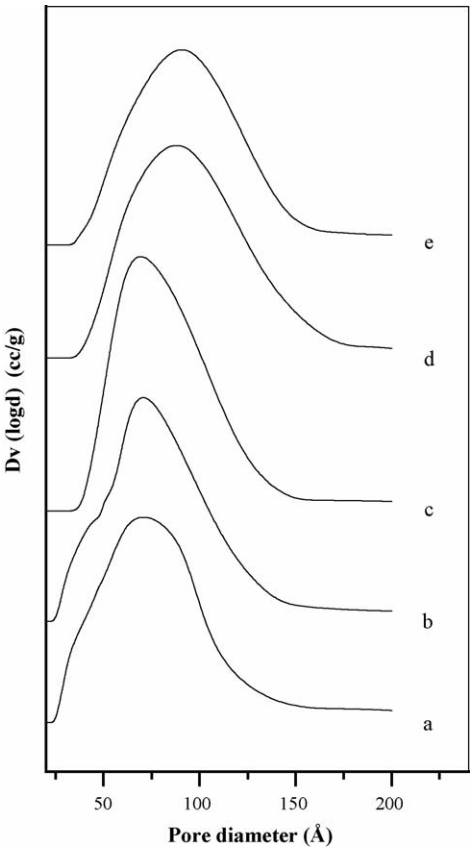

Fig. 3. BJH pore diameter of cobalt-containing mesoporous material: (a) HMS, (b) Co/HMS (1), (c) Co/HMS (2), (d) Co-HMS (100) and (e) Co-HMS (50).

corresponding textual parameters are given in Table 1 [11,12]. Isotherms of all samples show Type IV isotherm, according to IUPAC classification, at higher relative pressures (p/p_o), which is typical of mesoporous materials with one-dimensional cylindrical channels having bigger pore size [13]. Unlike MCM-41, the capillary condensation for the HMS samples was observed at higher relative pressure, indicating a pore enlargement and are consistent with the XRD results. Moreover, unlike the pore size distribution (PSD) curves obtained for M41S samples, the present HMS samples produce broad PSD curves. These structural differences show a different pore array for the HMS materials, prepared by the amine templated inorganic materials. In addition we observed that the pore size of Co-HMS samples are higher than pure HMS samples. Such kinds of results are noted for V-MCM-41 samples and are attributed to the substitution of vanadium in the frame wall positions [14]. Such a consideration in the present Co-HMS samples suggest that cobalt gets incorporated inside the framework and thereby enlarges its pore size. The surface area of pure HMS sample shows a high surface area of 503 $m^2\,g^{-1}$ and after cobalt substitution surface area gets increased to 538 $m^2\,g^{-1}$ for Co-HMS (100) and 618 $m^2\,g^{-1}$ for Co-HMS (50). However, as expected, the surface area of the grafted catalysts gets decreased and amounts to 96.4 and 92% for Co/HMS (1) and Co/HMS (2), respectively. This decrease in surface area may be due to the partial blockage of pores by forming cobalt oxide particles inside the pore channels by the post-synthesis method. However, these modifications had not changed the overall structural features of the material, as observed from the XRD and sorption isotherms.

3.3. Electron microscopy

Morphology as well as structural ordering of cobalt-containing HMS samples were analyzed by electron microscopy studies and are shown in Fig. 4. SEM picture of Co-HMS samples shows discrete spherical particles of diameter ~0.5–2 μm. Contrary, cobalt-grafted HMS samples show disordered spherical structures with the presence of agglomerated particles. Moreover, TEM images show the characteristic wormhole-like morphology for both the cobalt-containing samples [9]. Similar to SEM results, TEM images of cobalt-grafted samples also show the presence of agglomerated particles. Thus, the electronic microscopic studies show that the morphology of the HMS sample differs with the way of introduction of metal species inside the HMS matrix viz. direct synthesis and post-synthesis method.

3.4. Diffuse reflectance UV–vis spectra

Diffuse reflectance UV–vis spectroscopy is a powerful technique for gaining information about the coordination environment and oxidation states of metal species in various molecular sieves. Hence, to determine the coordination environment of

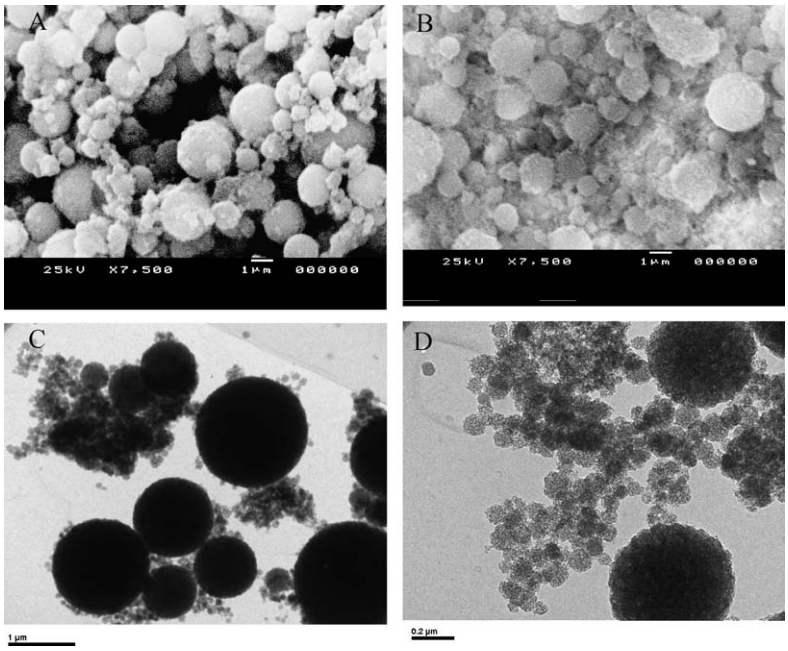

Fig. 4. SEM images of calcined cobalt-containing mesoporous: (A) Co-HMS (100), (B) Co/HMS (1); and TEM images of calcined cobalt-containing mesoporous (C) Co-HMS (100), (D) Co/HMS (1).

cobalt inside the HMS samples, DR UV–vis analyses was carried out in the range 12,000–35,000 cm^{-1} and are given in Fig. 5. Irrespective of the synthesis method, UV–vis analysis display an intense, three absorption maxima in the visible region. This triplet is assigned to the $^4A_2(F) \rightarrow {}^4T_1(P)$ transitions of high spin (d^7) Co^{2+} in tetrahedral position. This clearly indicates that cobalt is in the tetrahedral coordination with the support surface and the blue colour of the samples further supports this assignment [15–18]. For Co-HMS (50), a broad peak was observed around 27,000 cm^{-1} corresponding to the charge transfer bands of Co^{3+} in distorted tetrahedral position [19,23]. Moreover, it is apparent from Fig. 5 that the intensities of the triplet bands gets increased and broadened with an increase in the cobalt content. Bands above the 35,000 cm^{-1} are assigned to either charge transfer from O^{2-} to Co^{2+} or own absorption of molecular sieves [20–22].

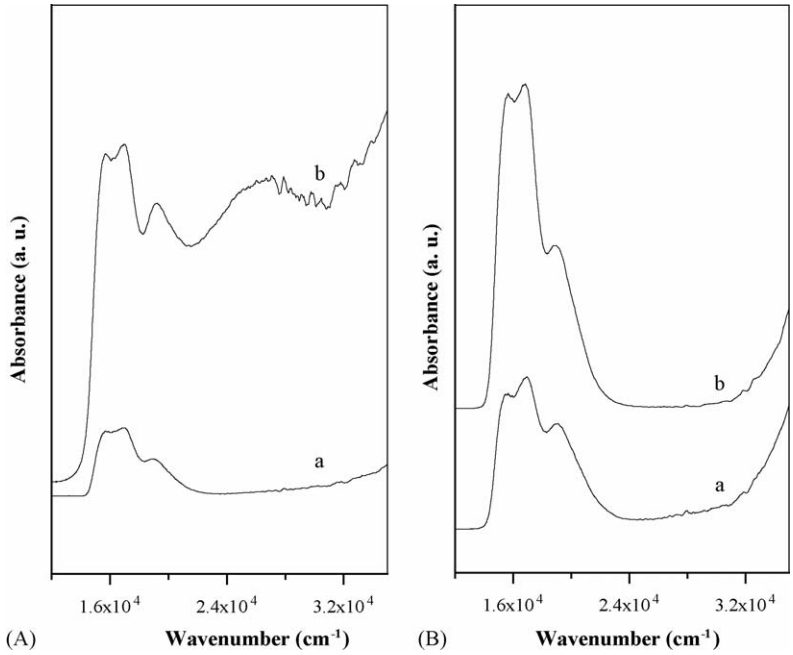

Fig. 5. Diffuse reflectance UV–vis spectra of cobalt-containing mesoporous materials: [A] (a) Co-HMS (100), (b) Co-HMS (50); [B] (a) Co/HMS (1), (b) Co/HMS (2).

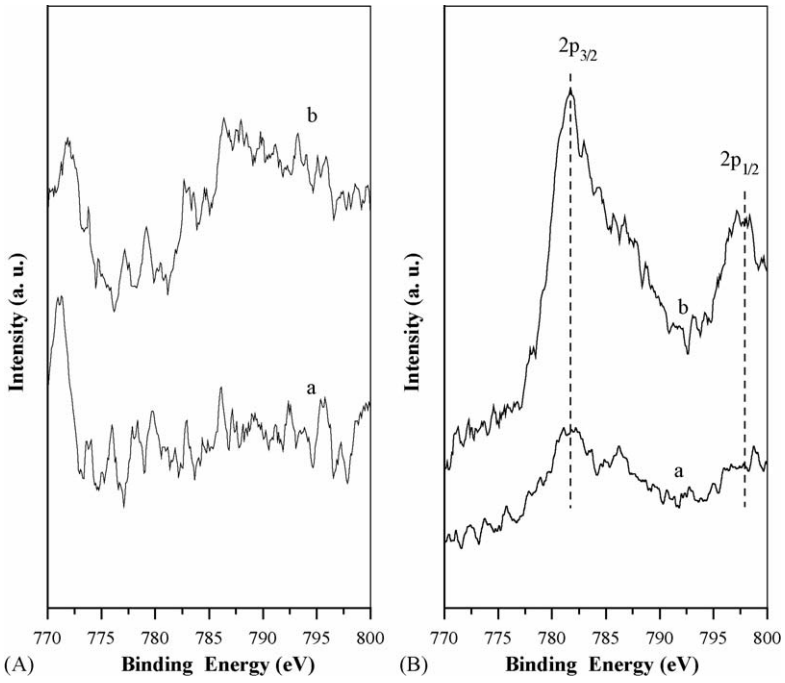

Fig. 6. XPS spectra of: [A] (a) Co-HMS (100), (b) Co-HMS (50); [B] (a) Co/HMS (1), (b) Co/HMS (2).

3.5. X-ray photoelectron spectra

XPS helps in the identification of oxidation state by exact measurement of peak positions and separation as well as from certain spectral features. X-ray photoelectron spectra of cobalt incorporated and grafted samples are shown in Fig. 6. For the grafted samples, the Co $2p_{3/2}$ transition peak occurs at 781.7 eV while $2p_{1/2}$ at 797.9 eV. With increase in the metal content, intensity of the $2p_{3/2}$ and $2p_{1/2}$ peaks was increased with some broadening. The energy difference between $2p_{1/2}$ and $2p_{3/2}$ peaks is 15.6 eV. It is close to that of Co^{2+} (16 eV) rather than Co^{3+} compounds (15.0 eV) [24,25]. This clearly indicates the presence of cobalt in +2 oxidation state which is in good agreement with the result from UV–vis spectra. Interestingly, the Co-HMS samples were devoid from the characteristic 2p peak ($2p_{1/2}$ and $2p_{3/2}$), which may be due to the fewer amounts of surface cobalt species in case of hydrothermally synthesized Co-HMS samples. However, for the grafted Co/HMS the percentage of the cobalt species detected is very high because of the post-synthesis grafting method. Since XPS is a surface technique, the present results suggest that more cobalt species resides on the support surface in Co/HMS samples, while since the cobalt gets substituted inside the framework for Co-HMS samples, they are not detectable by the XPS. Hence the Co $2p_{1/2}$ and $2p_{3/2}$ peaks are very prominent for the Co/HMS than Co-HMS samples, even though both the catalysts contain similar cobalt content.

3.6. Catalytic performance

In order to evaluate the catalytic activity of the cobalt-containing HMS samples, oxidation reaction of ethyl, benzene was carried out as a model reaction. Catalytic results show the formation of three oxidized products viz. benzaldehyde (BZ), acteophenone (AP) and benzoic acid (BA). The choice of the oxidant was *tert*-butyl hydroperoxide (TBHP) since aqu. hydrogen peroxide (H_2O_2) had not shown any conversion of the ethylbenzene.

In order to probe the role of solvents, series of solvent like CH_3CN, CH_2Cl_2, $(CH_3)_2CO$ and C_2H_5OH were used in the present reaction. When solvents were used for the oxidation of ethyl benzene, the conversions are less and follows the order CH_3CN (32.4) > CH_2Cl_2 (29.4) > $(CH_3)_2CO$ (12.8) > C_2H_5OH (0.8) and the selectivity towards the desired product acetophenone follows the order $(CH_3)_2CO$ (39.0) > CH_3CN (36.8) > CH_2Cl_2 (31.2) for Co-HMS(100), after 24 h of the reaction (Fig. 7B). Interestingly, the conversion was maximum under solvent free conditions for both the cobalt-containing samples Co-HMS (100) and Co/HMS (1) showed a maximum conversion of 49.5 and 39.0 wt%, respectively, after 24 h (Fig. 7B, Table 2). The selectivity towards acetophenone was found greater than 59% in absence of solvent over cobalt-containing HMS catalysts. The formation of other products viz. benzaldehyde may arise from the cleavage in the C–C bonds while the presence

Table 2
Catalytic activity of Co-HMS and Co/HMS for the oxidation of ethylbenzene

Entry	Catalyst	EB Conversion (wt%)	Selectivity (wt%)		
			BZ	AP	BA
1	HMS	0	–	–	–
2	Co-HMS (100)	49.5	25.0	60.0	15.0
3	Co-HMS (50)	36.9	21.7	59.2	18.5
4	Co/HMS (1)	39.0	37.2	65.4	14.0
5	Co/HMS (2)	35.0	34.8	63.3	15.0

Reaction conditions: ethylbenzene 1 g; TBHP 1.22 g; catalyst 0.05 g, temperature 80 °C; reaction time 24 h (absence of solvent).

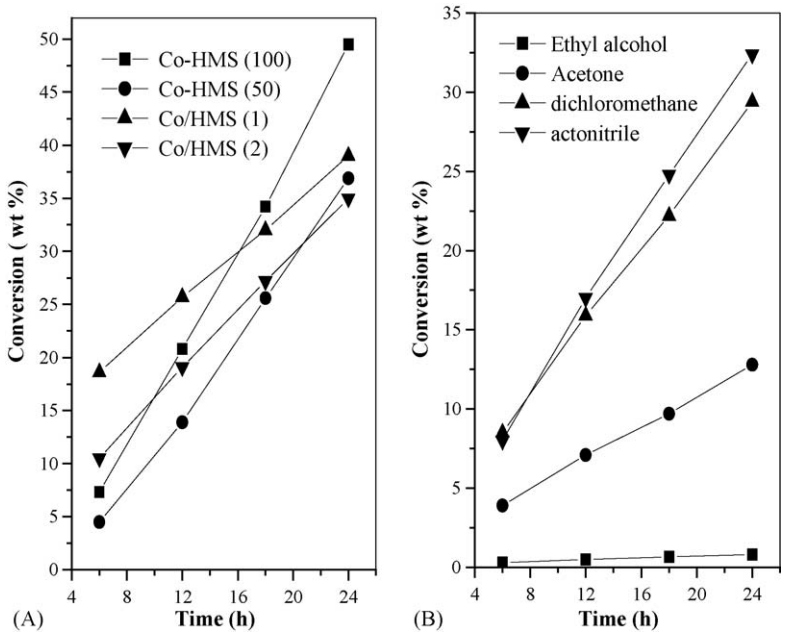

Fig. 7. [A] Conversion of ethylbenzene vs. time in solvent free media; [B] Influence of different solvent on catalytic activity for the catalyst Co-HMS (100).

of benzoic acid may results from the oxidation of benzaldehyde formed. Hence we suggest that solvent had negative impact over the performance of the cobalt-containing catalyst, which may possibly arise from the blocking of the active catalytic sites by the solvent molecules. Moreover, cobalt incorporated HMS samples (Co-HMS) shows a decrease in conversion with an increase in the cobalt content in the HMS matrix. The decreased conversion obtained for Co-HMS having lower Si/Co ratio may be due to the presence of nanosized cobalt particles that are unable to detect by the UV–vis and XPS techniques. Thus, the higher catalytic activity of Co-HMS (100) sample shows the well dispersion of cobalt in the framework and the presence of isolated cobalt sites are easily accessible for the substrate. In grafted cobalt samples also the conversion gets decreased with increasing the percentage of cobalt loading (1–2 wt%). Thus, the decreased conversions obtained at higher cobalt loadings can be ascribed to the formation of Co_3O_4 species, irrespective of the synthesis method.

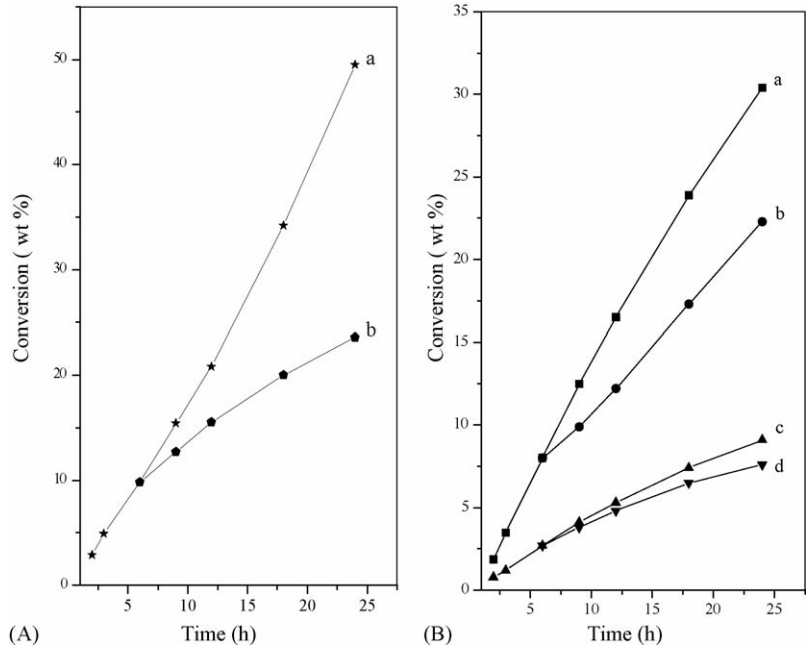

Fig. 8. Leaching study: [A] Conversion of ethylbenzene vs. time in absence of solvent for (a) Co-HMS (100) and (b) catalyst removed after 6h and filtrate was monitored for further reactions; [B] Conversion of ethylbenzene vs. time using acetonitrile as solvent for: (a) Co-HMS (100) and (b) Co-HMS (100) was removed and filtrate used after 6h, (c) Co/HMS (1) and (d) Co/HMS (1) was removed and filtrate used after 6h.

The heterogeneity of the catalyst was verified by performing the typical hot filtration experiments, under solvent free as well as in presence of solvents. The catalyst applied under the reaction condition was removed after 6 h catalytic run and the filtrate was monitored for further reactions. Interestingly, in the absence of solvent, conversion was not significantly enhanced after catalysts removal and shows a conversion of 23.6% after 24 h (Fig. 8A). However, in presence of acetonitrile solvent, the Co-HMS (100) and Co/HMS (1) catalysts show the leaching of active sites and among them the grafted catalyst shows an almost similar conversion like the fresh cycle (Fig. 8B). This result indicate that cobalt-containing catalyst are more stable under solvent free conditions and the catalyst prepared by direct hydrothermal methods shows limited leaching than the grafted catalysts. This finding is in contradiction to the earlier report, that leached cobalt species are not active in oxidation reactions [26].

4. Conclusion

Cobalt-containing hexagonal mesoporous molecular sieves were synthesized by direct hydrothermal and post-synthesis methods. The materials show the characteristic d_{100} reflection peak in the low angle and retain its structure and morphology after the introduction of cobalt in the support matrix. SEM and TEM images indicate agglomeration of particles after cobalt introduction by the post-synthesis grafting method. Diffuse reflectance UV–vis and XPS analysis had shown that cobalt is in the form of Co^{2+} cations having tetrahedral geometry. Catalytic activity of the developed cobalt-containing HMS catalysts in the liquid phase oxidation of ethylbenzene show that the direct hydrothermally synthesized catalysts are more active and stable than the cobalt grated catalysts. Moreover, the conversion and selectivity was found higher under lower cobalt concentrations as well as under solvent free conditions.

Acknowledgments

S.S. B. thanks to CSIR for granting research fellowship. The authors thank (Drs.) N.E. Jacob, S. Belhekar, R. Patil, Renu Pasricha and Mr. R. Shrivastav, N. Jha, Ms. S. Violet for their kind assistance in characterizing the catalysts and CSIR, New Delhi, for financial support (Task force project P23-CMM 0005B).

References

[1] C.T. Kresge, M.E. Leonowicz, W.J. Roth, J.C. Vartuli, J.S. Beck, Nature 359 (1992) 710.
[2] J.S. Beck, J.C. Vartuli, W.J. Roth, M.E. Leonowicz, C.T. Kresge, K.D. Schitt, C.T. Chu, D.H. Olson, E.W. Sheppard, B. McCullen, J.B. Higgins, J.L. Schelenker, J. Am. Chem. Soc. 114 (1992) 10834.
[3] P.T. Tanev, M. Chibwe, T.J. Pinnavaia, Nature 368 (1994) 321.
[4] (a) S.A. Bagshaw, E. Prouzet, T.J. Pinnavaia, Science 269 (1995) 1242; (b) G.S. Attard, J.C. Gyde, C.G. Goltner, Nature 378 (1995) 366.
[5] (a) E. Iglesia, S.C. Reyes, R.J. Modon, S.L. Soled, Adv. Catal. 39 (1993) 221;
(b) A.C. Vosloo, Fuel Process. Technol. 71 (2001) 149.
[6] S. Gontier, A. Tuel, Zeolites 15 (1995) 601.
[7] (a) J.S. Reddy, A. Sayari, Appl. Catal. A 148 (1996) 7;
(b) J.S. Reddy, A. Sayari, J. Chem. Soc. Chem. Commun. (1995) 2231.
[8] A. Tuel, S. Gontier, Chem. Mater. 8 (1996) 114.
[9] T.R. Pauly, T.J. Pinnavaia, Chem. Mater. 13 (2001) 987.
[10] P.T. Tanev, T.J. Pinnavaia, Chem. Mater. 8 (1996) 2068.
[11] E.P. Barrette, L.G. Joyner, P.P. Halenda, J. Am. Chem. Soc. 73 (1951) 373.
[12] S. Bruanaur, L.S. Deming, W.S. Deming, E.J. Teller, Am. Chem. Soc. 62 (1940) 1723.
[13] J.H. De Boer, in: D.H. Everette, F.S. Stone (Eds.), The Structure and Properties of Porous Materials, Butterworths, London, 1958, p. 68.
[14] S. Shylesh, A.P. Singh, J. Catal. 206 (2004) 230.
[15] D.L. Wood, J.P. Reimeka, J. Phys. Chem. 46 (1967) 3595.
[16] F.A. Cotton, G. Wilkinson, Advanced Inorganic Chemistry, Wiley, New York, 1980.
[17] A. Vinu, J. Dedecek, V. Murugesan, M. Hartmann, Chem. Mater. 14 (2002) 2433.
[18] A.A. Verberckmoes, M.G. Uytterhoeven, R.A. Schoonheydt, Microporous Mesoporous Mater. 22 (1998) 165.
[19] C. Montes, M.E. Davis, B. Murray, M. Narayana, J. Phys. Chem. 94 (1990) 6425.
[20] D. Kaucy, J. Dedecek, B. Wichterlova, Microporous Mesoporous Mater. 31 (1999) 75.
[21] J. Dedecek, D. Kaucy, B. Wichterlova, Microporous Mesoporous Mater. 483 (2000) 35.
[22] J. Dedecek, B. Wichterlova, J. Phys. Chem. B 103 (1999) 1462.
[23] A.A. Verberckmoes, M.G. Uytterhoeven, R.A. Schoonheydt, Microporous Mesoporous Mater. 22 (1998) 165.
[24] L. Guszi, D. Bazin, Appl. Catal. A 188 (1999) 163.
[25] G. Fierro, M.A. Eberrhardt, M. Houlla, D.M. Herculles, W.K. Hall, J. Phys. Chem. 100 (1996) 8468.
[26] W.A. Carvalho, M. Wallau, U. Schuchardt, J. Mol. Catal. A 144 (1999) 91.